

Nonadiabatic holonomic quantum computation on coupled transmons with ancillary

Tao Chen,¹ Jiang Zhang,² and Zheng-Yuan Xue^{1,*}

¹*Guangdong Provincial Key Laboratory of Quantum Engineering and Quantum Materials, and School of Physics and Telecommunication Engineering, South China Normal University, Guangzhou 510006, China*

²*State Key Laboratory of Low-Dimensional Quantum Physics and Department of Physics, Tsinghua University, Beijing 100084, China*

(Dated: January 15, 2022)

The physical implementation of holonomic quantum computation is challenging due to the needed complex controllable interactions on multilevel quantum systems. Here we propose to implement the nonadiabatic holonomic quantum computation with the conventional capacitive coupled superconducting transmon qubits, where a universal set of quantum gates is constructed with the help of the interaction to an auxiliary qubit rather than consulting to delicate control over an auxiliary level of multilevel quantum systems. Explicitly, these quantum gates are realized by tunable interactions in an all-resonant way, which leads to high-fidelity gate operations. In this way, the distinct merit of our scheme is that we only use the two lowest levels of a transmon to form the qubit states. In addition, the auxiliary qubits are in their ground states before and after every gate operation. Therefore, our scheme paves a promising way towards the practical realization of high-fidelity nonadiabatic holonomic quantum computation.

I. INTRODUCTION

Quantum computers are believed to outperform its classical counterparts in solving certain hard problems [1]. However, quantum states are susceptible to noises induced by their surrounding environment, thus the practical implementation of quantum computers is harsh. Since geometric phases only depend on the global properties of the evolution paths, they can effectively resist the influence of certain local noises and thus become a promising medium for quantum computation. Holonomic quantum computation (HQC) [2] is a strategy to build universal set of robust gates using non-Abelian geometric phases [3]. This idea is originally proposed based on adiabatic evolution [4–8] which aims to achieve high-fidelity quantum computation. However, the adiabatic condition requires long evolution time, where environmental noises will ruin the wanted operation.

For practical quantum computation, nonadiabatic evolution is necessary [9, 10]. Recently, nonadiabatic HQC has been proposed by using the cyclic evolutions of a subspace existing in the general three-level Λ quantum system, so that a universal set of fast geometric quantum gates can be implemented [11–24]. Due to its experimental feasibility, this type of nonadiabatic gates has been experimentally demonstrated on superconducting circuits [25–28], NMR [29, 30], and electron spins in diamond [31–34].

The above nonadiabatic HQC schemes based on three-level systems require the use of a third auxiliary energy level. This is challenging for superconducting transmon qubits, the energy spectrum of which is only weakly anharmonic, and thus makes the implementation of the needed complex controllable interactions between qubits to be difficult. In addition, problems will occur when this implementation approach applies to certain quantum operations with encoding which are indispensable part of quantum computation. Since the required projective measurement on the multilevel quantum systems

can have a state collapse to the auxiliary level, in addition to the levels used for a qubit. In order to avoid this drawback, we propose to realize the nonadiabatic HQC schemes [35–38] with capacitive coupled superconducting qubits, where we construct universal holonomic gates with the help of auxiliary qubits rather than auxiliary levels. The distinct merit of our scheme is that the auxiliary qubits are in their ground state before and after each gate operation so that the problem caused by auxiliary level can be overcome. In addition, our scheme uses the two lowest levels of a transmon to form the qubit states and can result in universal HQC with conventional resonant interactions, leading to fast and high-fidelity universal quantum gates. Moreover, to obtain tunable all-resonant interaction between the target and auxiliary qubits, we only need to add modulations on the target qubits by well-controlled microwaves. Therefore, our scheme can be readily implemented in the coupled superconducting qubits 2D lattice, and thus offers promising scalability.

II. ARBITRARY SINGLE-QUBIT GATES

The setup we consider is a scalable coupled superconducting qubits chain illustrated in Fig. 1(a), which is a arbitrary section of the coupled superconducting qubits 2D lattice. It consists of superconducting transmon qubits [39] with different frequencies. In order to realize arbitrary single-qubit holonomic gates on a target transmon qubit A, we introduce an auxiliary transmon qubit B which is driven by a classical field and capacitively coupled to the transmon qubit A as shown in Fig. 1(b). Furthermore, we consider the realistic case of the transmon qubit, i.e., it is weakly anharmonic, so that we need to take the third energy level that is beyond the qubit states into account, since the main leakage out of the qubit basis comes from this level. Assuming $\hbar = 1$ hereafter, the Hamiltonian of the coupled system can be expressed as

$$H_{c1} = \sum_{\chi=A,B} \omega_{\chi} n_{\chi} + \frac{\alpha_{\chi}}{2} (1 - n_{\chi}) n_{\chi} + g_{AB} (a^{\dagger} b + a b^{\dagger}) + \varepsilon \cos(\omega t - \phi) (b^{\dagger} + b), \quad (1)$$

* zyxue83@163.com

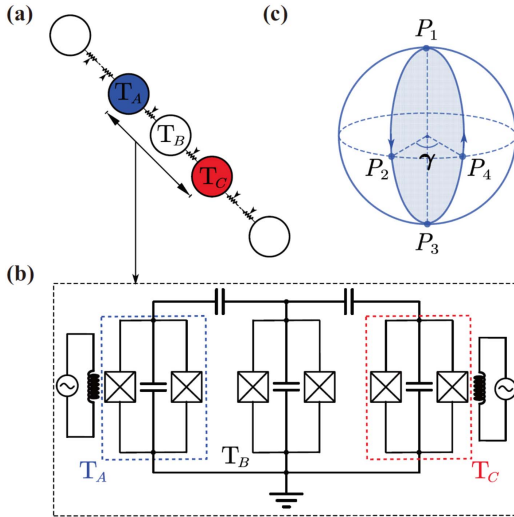


FIG. 1. The proposed setup of our scheme. (a) The configuration of the coupled superconducting qubits chain, where the circles denote transmon qubits with different frequencies. (b) The interactions between two transmon qubits A with B, and B with C, adding different periodical modulations to transition frequency of the target transmon qubit A and C by a pair of well-controlled microwaves, respectively. (c) The orange-slice-shaped evolution path in Bloch sphere.

where $n_A = a^\dagger a$, $n_B = b^\dagger b$ with $a = |0\rangle_A \langle 1| + \sqrt{2}|1\rangle_A \langle 2|$ and $b = |0\rangle_B \langle 1| + \sqrt{2}|1\rangle_B \langle 2|$ being the standard lower operators for the transmon qubit A and B. ω_A and ω_B are the associated transition frequencies with α_A and α_B being the intrinsic anharmonicity of the transmon qubit A and B, respectively. g_{AB} is the qubit-qubit interaction coupling strength, and ε , ω and ϕ are the classical driving strength, frequency and phase on the transmon qubit B, respectively.

Usually, two transmon qubits A and B do not have identical energy splitting, we add an parametric driving on transmon qubit A to induce effectively resonant coupling between two transmon qubits [40–43], which can be realized by adding an ac magnetic flux through the transmon qubit A loop. In this way, a periodical modulation of the transmon qubit A's transition frequency of

$$\omega_A(t) = \omega_A + \epsilon_1 \sin(\nu_1 t + \pi/2) \quad (2)$$

can be achieved. Moving into the interaction picture, the interaction Hamiltonian reduces to

$$\begin{aligned} H_I = & g_{AB} \left\{ |10\rangle \langle 01| e^{-i\Delta_1 t} e^{-i\beta_1 \cos(\nu_1 t + \pi/2)} \right. \\ & + \sqrt{2}|11\rangle \langle 02| e^{-i(\Delta_1 - \alpha_B)t} e^{-i\beta_1 \cos(\nu_1 t + \pi/2)} \\ & + \sqrt{2}|20\rangle \langle 11| e^{-i(\Delta_1 + \alpha_A)t} e^{-i\beta_1 \cos(\nu_1 t + \pi/2)} \left. \right\} \\ & + \frac{\varepsilon}{2} \sum_{j=0,1} \sqrt{j+1} |j+1\rangle_B \langle j| e^{i(\delta - j\alpha_B)t} e^{i\phi} + \text{H.c.}, \end{aligned} \quad (3)$$

where $\Delta_1 = \omega_B - \omega_A$, $\delta = \omega_B - \omega$, $\beta_1 = \epsilon_1/\nu_1$, and $|mn\rangle = |m\rangle_A \otimes |n\rangle_B$. We consider the case of resonant driven on the transmon qubit B, i.e., $\delta = 0$, and the parametric driving compensate the energy difference between transmon qubit A

and B, i.e., $\Delta_1 = \nu_1$. Then, using the Jacobi-Anger identity

$$e^{-i\beta_1 \cos(\nu_1 t + \pi/2)} = \sum_{m=-\infty}^{\infty} (-i)^m J_m(\beta_1) e^{-im(\nu_1 t + \pi/2)},$$

with $J_m(\beta_1)$ being Bessel functions of the first kind. Applying the rotating-wave approximation by neglecting the high-order oscillating terms, we obtain an effective resonant interaction Hamiltonian as

$$H_1 = g'_{AB} |10\rangle \langle 01| + \frac{\varepsilon}{2} |1\rangle_B \langle 0| e^{i\phi} + \text{H.c.}, \quad (4)$$

where $g'_{AB} = J_1(\beta_1)g_{AB}$.

By setting parameters $g'_{AB} = \Omega \cos(\theta/2)$, $\varepsilon = \Omega \sin(\theta/2)$ with $\Omega = \sqrt{g_{AB}^2 + \varepsilon^2}$ and $\theta = 2 \tan^{-1}(\varepsilon/g'_{AB})$, the interaction Hamiltonian can be reduced to the following block off-diagonal form

$$H_1 = \Omega \begin{pmatrix} 0 & F \\ F^\dagger & 0 \end{pmatrix}, \quad (5)$$

in the ordered orthonormal basis $S = \{|00\rangle, |10\rangle, |01\rangle, |11\rangle\}$ with

$$F = \begin{pmatrix} \frac{1}{2} \sin \frac{\theta}{2} e^{-i\phi} & 0 \\ \cos \frac{\theta}{2} & \frac{1}{2} \sin \frac{\theta}{2} e^{-i\phi} \end{pmatrix}. \quad (6)$$

We find matrix F is complex-valued and time-independent, and it satisfies the condition of $\det F \neq 0$. Therefore, matrix F is invertible, and has a unique singular value decomposition of matrix $F = WDR^\dagger$, where

$$\begin{aligned} W &= \begin{pmatrix} \sin \frac{\theta}{4} & \cos \frac{\theta}{4} e^{-i\phi} \\ \cos \frac{\theta}{4} e^{i\phi} & -\sin \frac{\theta}{4} \end{pmatrix}, \\ D &= \begin{pmatrix} \cos^2 \frac{\theta}{4} & 0 \\ 0 & \sin^2 \frac{\theta}{4} \end{pmatrix}, \\ R^\dagger &= \begin{pmatrix} \cos \frac{\theta}{4} & \sin \frac{\theta}{4} e^{-i\phi} \\ \sin \frac{\theta}{4} e^{i\phi} & -\cos \frac{\theta}{4} \end{pmatrix}, \end{aligned} \quad (7)$$

respectively.

We can separate the four-dimensional Hilbert space of the Hamiltonian H_1 in Eq. (5), into two two-dimensional subspaces,

$$S = S_0 \oplus S_1 \quad (8)$$

where $S_0 = \text{Span}\{|00\rangle, |10\rangle\}$, and $S_1 = \text{Span}\{|01\rangle, |11\rangle\}$. This implies that in the basis S the time evolution operator splits into 2×2 blocks. The final time evolution operator can be expressed as

$$U_1(\tau) = \begin{pmatrix} W \cos(a_\tau D) W^\dagger & -iW \sin(a_\tau D) R^\dagger \\ -iR \sin(a_\tau D) W^\dagger & R \cos(a_\tau D) R^\dagger \end{pmatrix}, \quad (9)$$

where $a_\tau = \Omega\tau$ with τ being the total evolution time.

We now explain how the four-dimensional model can be used to achieve arbitrary single-qubit holonomic gates on target transmon qubit A, through the orange-slice-shaped evolution path [36, 44, 45], as shown in Fig. 1(c). Define $F_1 = W_1 D_1 R_1^\dagger$ and $\phi = 0$ in the first path segment $[0, \frac{\tau}{2}]$.

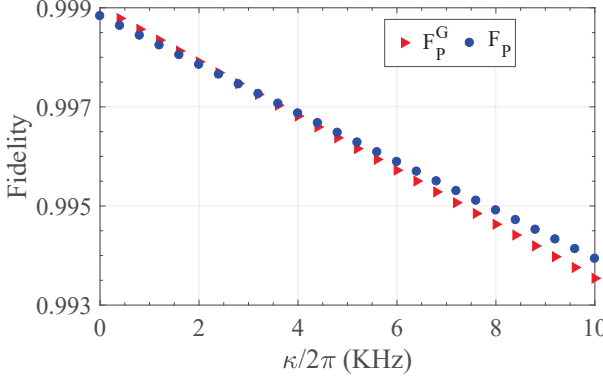


FIG. 2. The state fidelity F_P of the phase-shift gate with the initial state being $\frac{1}{\sqrt{2}}(|00\rangle + |10\rangle)$ and the gate fidelity F_P^G as a function of the different decoherence rates.

Starting from the subspace S_0 at point P_1 , reaching the subspace S_1 via path $P_1 \rightarrow P_2 \rightarrow P_3$ by choosing a certain time such that $\cos(a_{\frac{\tau}{2}} D_1) = 0$ and $\sin(a_{\frac{\tau}{2}} D_1) = G_i$, where $i = I$ or z , $G_I = \text{diag}\{1, 1\}$, $G_z = \text{diag}\{1, -1\}$. We note that, in order to satisfy above equality constraint, one needs to limit the parameter $\theta \neq 2n\pi$ where n is an integer. At point P_3 in Bloch sphere, we only change the relative phase parameter $\phi = \gamma$. Similarly, we define $F_2 = W_2 D_2 R_2^\dagger$ in the second path segment $[\frac{\tau}{2}, \tau]$. And then returns to the initial subspace S_0 via path $P_3 \rightarrow P_4 \rightarrow P_1$ by choosing a certain time such that $\cos(a_{\frac{\tau}{2}} D_2) = 0$, $\sin(a_{\frac{\tau}{2}} D_2) = G_i$. The final choice of i depends on the parameters θ, ϕ and a_τ . We obtain the time evolution operator as

$$U_1(\tau) = U\left(\tau, \frac{\tau}{2}\right) U\left(\frac{\tau}{2}, 0\right) = U_0 \otimes |0\rangle_B \langle 0| + U_1 \otimes |1\rangle_B \langle 1|, \quad (10)$$

where the evolution operator $U_0 = -W_2 G_i R_2^\dagger R_1 G_i W_1^\dagger$ and $U_1 = -R_2 G_i W_2^\dagger W_1 G_i R_1^\dagger$ act on the target transmon qubit A conditionalized on the states $|0\rangle_B$ and $|1\rangle_B$ of the auxiliary transmon qubit B, respectively. If we initially prepare the auxiliary transmon qubit B in its ground state $|0\rangle_B$, we select the evolution operator U_0 in the orthogonal subspace $S_0 = \{|00\rangle, |10\rangle\}$. We further set $G_i \equiv G_I = \text{diag}\{1, 1\}$ and $\gamma = \pi$, the time evolution operator on transmon qubit A is

$$U'_0 = \begin{pmatrix} \cos \theta & -\sin \theta \\ \sin \theta & \cos \theta \end{pmatrix} = e^{-i\theta\sigma_y}, \quad (11)$$

which is a rotation matrix around the Y-axis by an angle θ . Alternatively, if we take $G_i \equiv G_z = \text{diag}\{1, -1\}$, the time evolution operator becomes

$$U''_0 = \begin{pmatrix} e^{-i\gamma} & 0 \\ 0 & e^{i\gamma} \end{pmatrix} = e^{-i\gamma\sigma_z}, \quad (12)$$

which is a rotation matrix around the Z-axis by an angle γ .

The above processes are nonadiabatic holonomy transformations, because the following two conditions are satisfied: (i) The Hamiltonian H_1 vanishes in the evolving subspace S_0 , i.e.,

$$P_0 H_1 P_0 = U_1(t) P_0 H_1 P_0 U_1^\dagger(t) = 0 \quad (13)$$

where $P_0 = |00\rangle\langle 00| + |10\rangle\langle 10|$. It shows that the evolution satisfies the parallel-transport condition; (ii) The evolution of the subspace S_0 is cyclic, since

$$\begin{aligned} S_0(\tau) &\equiv \text{Span}\{U_1(\tau)|00\rangle, U_1(\tau)|10\rangle\} \\ &= \text{Span}\{|00\rangle, |10\rangle\} = S_0 \end{aligned} \quad (14)$$

Thus, an arbitrary single-qubit holonomic gate on target transmon qubit A can be implemented.

However, for practical physical implementations, the decoherence is unavoidable. Therefore, we consider the decoherence effect by numerical simulating the following Lindblad master equation,

$$\begin{aligned} \dot{\rho}_1 &= -i[H_{c1}, \rho_1] + \sum_{\chi=A, B} \left\{ \frac{\kappa_\chi^\chi}{2} \mathcal{L}(|0\rangle_\chi \langle 1| + 2|1\rangle_\chi \langle 2|) \right. \\ &\quad \left. + \frac{\kappa_z^\chi}{2} \mathcal{L}(|1\rangle_\chi \langle 1| + 2|2\rangle_\chi \langle 2|) \right\}, \end{aligned} \quad (15)$$

where ρ_1 is the density matrix of the transmon qubit A, $\mathcal{L}(\mathcal{A}) = 2\mathcal{A}\rho_1\mathcal{A}^\dagger - \mathcal{A}^\dagger\mathcal{A}\rho_1 - \rho_1\mathcal{A}^\dagger\mathcal{A}$ is the Lindblad operator for operator \mathcal{A} , and κ_χ^χ , κ_z^χ are the relaxation and dephasing rates of the transmon qubits, respectively. According to recent superconducting qubit experiments, we choose $\alpha_A = 2\pi \times 375$ MHz, $\alpha_B = 2\pi \times 350$ MHz [46], $\Delta_1 = 2\pi \times 245$ MHz [42], $\beta_1 = \epsilon_1/\nu_1 = \epsilon_1/\Delta_1 \simeq 1.6$, $\Omega = 2\pi \times 13$ MHz can be reached by $g_{AB} = 2\pi \simeq 11.41$ MHz and $\varepsilon = 2\pi \simeq 11.26$ MHz. As demonstrated in Ref. [47], the relaxation and dephasing rates of a transmon qubit are on the same order, about $2\pi \times 1.5$ KHz. Here, we assume that the relaxation and dephasing rates of the transmon qubits are the same, i.e., $\kappa_-^A = \kappa_z^A = \kappa_-^B = \kappa_z^B = \kappa$ being $2\pi \times [0, 10]$ KHz. We take the phase-shift gate $U_P = \text{diag}\{1, e^{i\frac{\pi}{4}}\}$ as an example which corresponds to $\gamma = \pi/8$ in Eq. (13). Assuming that the initial state of two-qubit is $\frac{1}{\sqrt{2}}(|00\rangle + |10\rangle)$, the phase-shift gate results in the ideal final state $|\psi_{f_P}\rangle = \frac{1}{\sqrt{2}}(|00\rangle + e^{i\frac{\pi}{4}}|10\rangle)$. We first evaluate the performance of this gate by the state fidelity defined by $F_P = \langle\psi_{f_P}|\rho_1|\psi_{f_P}\rangle$. In Fig. 2, we use blue circles to show the trend of the state fidelity with the decoherence rates κ , and find that the state fidelity can reach about 99.64% for $\kappa = 2\pi \times 5$ KHz. Moreover, to fully evaluate the gate, for a general initial state $|\psi_i\rangle = \cos \theta_i |00\rangle + \sin \theta_i |10\rangle$, U_P results in an ideal final state $|\psi_f\rangle = \cos \theta_i |00\rangle + e^{i\frac{\pi}{4}} \sin \theta_i |10\rangle$, we define the gate fidelity as $F_P^G = \frac{1}{2\pi} \int_0^{2\pi} \langle\psi_f|\rho_1|\psi_f\rangle d\theta_1$ [48] with the integration is numerically done for 1000 input states with θ' uniformly distributed over $[0, 2\pi]$. In Fig. 2, we plot the gate fidelity as a function of the decoherence rates κ with red triangles. We find that the gate fidelity is also about 99.63% for $\kappa = 2\pi \times 5$ KHz, which is experimentally accessible. Finally, we want to emphasise that all the simulation hereafter is based on the original interaction Hamiltonian without any approximation, which thus also verify our analytical results.

III. NONTRIVIAL TWO-QUBIT GATES

Next we consider the construction of a nontrivial two-qubit holonomic gate on a pair of target qubits in a coupled super-

conducting qubits chain. Obviously, our scheme can also be implemented in the coupled superconducting qubits 2D lattice because the coupled superconducting qubits chain is part of it. Combining with the implemented arbitrary single-qubit holonomic gates, nonadiabatic holonomic quantum computation can then be realized. As shown in Fig. 1(a), both two target transmon qubits A and C are coupled to the auxiliary transmon qubit B. This three-qubit system is described by

$$H_{c2} = \sum_{\chi=A,B,C} \omega_\chi n_\chi + \frac{\alpha_\chi}{2} (1 - n_\chi) n_\chi + g_{AB} (a^\dagger b + a b^\dagger) + g_{BC} (b^\dagger c + b c^\dagger). \quad (16)$$

To get the resonant interactions among three transmon qubits, we add two different parametric modulations to the transition frequency of transmon qubit A and C by two well-controlled microwaves, which are

$$\begin{aligned} \omega_A(t) &= \omega_A + \epsilon_1 \sin(\nu_1 t + \pi/2), \\ \omega_C(t) &= \omega_C + \epsilon_2 \sin(\nu_2 t + \varphi + \pi/2). \end{aligned} \quad (17)$$

We set $\Delta_1 = \nu_1$ and $\Delta_2 = \omega_B - \omega_C = \nu_2$. Applying the rotating-wave approximation by neglecting the oscillating terms, and the finally effective resonant interaction Hamiltonian reads

$$H_2 = g'_{AB} |01\rangle_{AB} \langle 10| + g'_{BC} e^{i\varphi} |01\rangle_{BC} \langle 10| + \text{H.c.}, \quad (18)$$

where $g'_{AB} = J_1(\beta_1)g_{AB}$, $\beta_1 = \epsilon_1/\nu_1$ and $g'_{BC} = J_1(\beta_2)g_{BC}$, $\beta_2 = \epsilon_2/\nu_2$.

Next, we proceed to explain how the above effective resonant interaction Hamiltonian can be used to achieve non-trivial two-qubit holonomic gates on target transmon qubits A and C. Resetting $g'_{AB} = g \cos(\vartheta/2)$, $g'_{BC} = g \sin(\vartheta/2)$ with $g = \sqrt{g_{AB}^2 + g_{BC}^2}$ and $\vartheta = 2 \tan^{-1}(g'_{BC}/g'_{AB})$, the Hamiltonian can be reduced to the following block off-diagonal form

$$H_2 = g(|0\rangle_B \langle 1| \otimes K + |1\rangle_B \langle 0| \otimes K^\dagger), \quad (19)$$

where

$$K = \begin{pmatrix} 0 & 0 & 0 & 0 \\ \sin \frac{\vartheta}{2} e^{i\varphi} & 0 & 0 & 0 \\ \cos \frac{\vartheta}{2} & 0 & 0 & 0 \\ 0 & \cos \frac{\vartheta}{2} & \sin \frac{\vartheta}{2} e^{i\varphi} & 0 \end{pmatrix} \quad (20)$$

is within the four-dimensional orthonormal basis $\{|00\rangle_{AC}, |01\rangle_{AC}, |10\rangle_{AC}, |11\rangle_{AC}\}$. We perform a unique singular value decomposition on matrix K in the form of

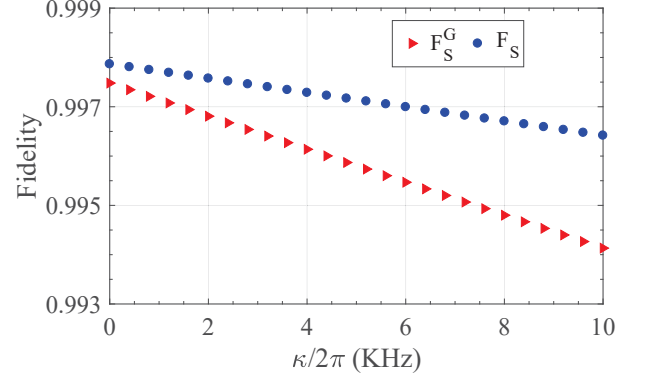


FIG. 3. The state-fidelity F_S of the SWAP-like two-qubit gate with the initial state being $\frac{1}{\sqrt{2}}(|000\rangle + |001\rangle)$ and the gate fidelity F_S^G as a function of the decoherence rates.

$K = XYZ^\dagger$ with

$$\begin{aligned} X &= \begin{pmatrix} 1 & 0 & 0 & 0 \\ 0 & \cos \frac{\vartheta}{2} & 0 & \sin \frac{\vartheta}{2} e^{i\varphi} \\ 0 & -\sin \frac{\vartheta}{2} e^{-i\varphi} & 0 & \cos \frac{\vartheta}{2} \\ 0 & 0 & 1 & 0 \end{pmatrix}, \\ Y &= \begin{pmatrix} 0 & 0 & 0 & 0 \\ 0 & 0 & 0 & 0 \\ 0 & 0 & 1 & 0 \\ 0 & 0 & 0 & 1 \end{pmatrix}, \\ Z^\dagger &= \begin{pmatrix} 0 & 0 & 0 & 1 \\ 0 & \sin \frac{\vartheta}{2} e^{-i\varphi} & -\cos \frac{\vartheta}{2} & 0 \\ 0 & \cos \frac{\vartheta}{2} & \sin \frac{\vartheta}{2} e^{i\varphi} & 0 \\ 1 & 0 & 0 & 0 \end{pmatrix}. \end{aligned} \quad (21)$$

In the same way say in the single qubit gate case, we separate the eight-dimensional three-qubits Hilbert space of the Hamiltonian H_2 into two four-dimensional subspaces, i.e.,

$$M = M_0 \oplus M_1 \quad (22)$$

where $M_0 = \text{Span}\{|000\rangle, |001\rangle, |100\rangle, |101\rangle\}$ and $M_1 = \text{Span}\{|010\rangle, |011\rangle, |110\rangle, |111\rangle\}$, with $|ijk\rangle \equiv |i\rangle_A \otimes |j\rangle_B \otimes |k\rangle_C$. Similarly, in the basis M the time evolution operator splits into 4×4 blocks, and the time evolution operator can be expressed as

$$U_2(T) = \begin{pmatrix} X \cos(b_T Y) X^\dagger & -iX \sin(b_T Y) Z^\dagger \\ -iZ \sin(b_T Y) X^\dagger & Z \cos(b_T Y) Z^\dagger \end{pmatrix} \quad (23)$$

where $b_T = gT$ with T being the evolution time. By choosing a certain time such that $\cos(b_T Y) = J = \text{diag}\{1, 1, -1, -1\}$ and $\sin(b_T Y) = \text{diag}\{0, 0, 0, 0\}$, we can obtain

$$U_2(T) = V_0 \otimes |0\rangle_B \langle 0| + V_1 \otimes |1\rangle_B \langle 1|, \quad (24)$$

where the evolution operator $V_0 = X J X^\dagger$ and $V_1 = Z J Z^\dagger$ act on the target transmon qubits A and C conditionalized on the states $|0\rangle_B$ and $|1\rangle_B$ of the auxiliary transmon qubit B, respectively. The above obtained evolution operator is of the holonomic nature, because the following two conditions can

be satisfied. (i) Due to $[H_2, U_2(t)] = 0$, the Hamiltonian H_2 vanishes on evolving subspace M_0 , i.e.,

$$L_0 H_2 L_0 = U_2(t) L_0 H_2 L_0 U_2^\dagger(t) = 0 \quad (25)$$

with $L_0 = |000\rangle\langle 000| + |001\rangle\langle 001| + |100\rangle\langle 100| + |101\rangle\langle 101|$. (ii) The evolution of the orthogonal subspaces M_0 also undergoes cyclic evolution, since

$$\begin{aligned} M_0(T) &\equiv \text{Span}\{U_2(T)|000\rangle, U_2(T)|001\rangle, \\ &\quad U_2(T)|100\rangle, U_2(T)|101\rangle\} \\ &= \text{Span}\{|000\rangle, |001\rangle, |100\rangle, |101\rangle\} = M_0 \end{aligned} \quad (26)$$

The similar discussion is available for evolving subspace M_1 .

Then, initially prepare the auxiliary transmon qubit B in $|0\rangle_B$, i.e., selecting the evolution operator V_0 in orthogonal subspace $M_0 = \text{Span}\{|000\rangle, |001\rangle, |100\rangle, |101\rangle\}$, we can obtain the nontrivial two-qubit holonomic gates as

$$\begin{aligned} V_0 &= X \times \text{diag}\{1, 1, -1, -1\} \times X^\dagger \\ &= \begin{pmatrix} 1 & 0 & 0 & 0 \\ 0 & \cos \vartheta & -\sin \vartheta e^{i\varphi} & 0 \\ 0 & -\sin \vartheta e^{-i\varphi} & -\cos \vartheta & 0 \\ 0 & 0 & 0 & -1 \end{pmatrix}, \end{aligned} \quad (27)$$

on the target transmon qubits A and C. Such as tuning the parameters φ and ϑ from the external modulations as $\varphi = \pi$ and $\vartheta = \pi/2$, we can get a SWAP-like two-qubit gate [49]

$$V_S = \begin{pmatrix} 1 & 0 & 0 & 0 \\ 0 & 0 & 1 & 0 \\ 0 & 1 & 0 & 0 \\ 0 & 0 & 0 & -1 \end{pmatrix}, \quad (28)$$

which is a nontrivial two-qubit gate for quantum computation.

We next take this SWAP-like gate as an example to verify the performance of two-qubit gates. Here we set $\Delta_1 = 2\pi \times 245$ MHz, $\Delta_2 = 2\pi \times 230$ MHz, and $\beta_1 = \beta_2 \simeq 1.6$. Set the

value of anharmonicity $\alpha_C = 2\pi \times 310$ MHz and the coupling strength $g_{AB} = g_{BC} \simeq 2\pi \times 11.41$ MHz. Suppose the initial state of three-qubit is $\frac{1}{\sqrt{2}}(|000\rangle + |001\rangle)$ which results in the ideal final state $|\psi_{f_S}\rangle = \frac{1}{\sqrt{2}}(|000\rangle + |100\rangle)$. Here we evaluate this gate by the state fidelity defined by $F_S = \langle \psi_{f_S} | \rho_2 | \psi_{f_S} \rangle$. In order to fully evaluate the performance of the implemented two-qubit gate, for a general initial state $|\psi_2\rangle = (\cos \vartheta_1 |0\rangle_A + \sin \vartheta_1 |1\rangle_A) \otimes |0\rangle_B \otimes (\cos \vartheta_2 |0\rangle_C + \sin \vartheta_2 |1\rangle_C)$ and ideal final state $|\psi_f\rangle = V_S |\psi_2\rangle$, we define the two-qubit gate fidelity as $F_S^G = \frac{1}{4\pi^2} \int_0^{2\pi} \int_0^{2\pi} \langle \psi_f | \rho_2 | \psi_f \rangle d\vartheta_1 d\vartheta_2$. In Fig. 3, we plot the state and gate fidelities as a function of the decoherence rates κ , respectively represented by blue circles and red triangles, where gate fidelity of 99.41% can be achieved when $\kappa/2\pi = 10$ KHz. Note that the best two qubit gate fidelity [50] is 99.40% for decay rates around 4 KHz.

IV. CONCLUSION

In summary, we have proposed to implement the nonadiabatic HQC scheme in a coupled superconducting qubits system. Through the control of the amplitudes and relative phases of driving ac magnetic modulating flux, fast and high-fidelity universal quantum gates on target transmon qubits can be obtained, in a tunable and all-resonant way. Thus, our scheme provides a promising way towards the practical realization of high-fidelity nonadiabatic HQC.

ACKNOWLEDGMENTS

This work was supported in part by the National Natural Science Foundation of China and the National Key R&D Program of China (Grant No. 2016YFA0301803).

[1] P. W. Shor, SIAM Rev. **41**, 303 (1999).
[2] P. Zanardi and M. Rasetti, Phys. Lett. A **264**, 94 (1999).
[3] F. Wilczek and A. Zee, Phys. Rev. Lett **52**, 2111 (1984).
[4] J. Pachos, P. Zanardi, and M. Rasetti, Phys. Rev. A **61**, 010305 (1999).
[5] L.-M. Duan, J. I. Cirac, and P. Zoller, Science **292**, 1695 (2001).
[6] P. Zhang, Z. D. Wang, J. D. Sun, and C. P. Sun, Phys. Rev. A **71**, 042301 (2005).
[7] I. Kamleitner, P. Solinas, C. Müller, A. Shnirman, and M. Möttönen, Phys. Rev. B **83**, 214518 (2011).
[8] V. V. Albert, C. Shu, S. Krastanov, C. Shen, R.-B. Liu, Z.-B. Yang, R. J. Schoelkopf, M. Mirrahimi, M. H. Devoret, and L. Jiang, Phys. Rev. Lett. **116**, 140502 (2016).
[9] S.-L. Zhu and Z. D. Wang, Phys. Rev. Lett **89**, 097902 (2002).
[10] S.-L. Zhu and Z. D. Wang, Phys. Rev. A **67**, 022319 (2003).
[11] E. Sjöqvist, D. M. Tong, L. M. Andersson, B. Hessmo, M. Johansson, and K. Singh, New J. Phys. **14**, 103035 (2012).
[12] G. F. Xu, J. Zhang, D. M. Tong, E. Sjöqvist, and L. C. Kwek, Phys. Rev. Lett. **109**, 170501 (2012).
[13] J. Zhang, L.-C. Kwek, E. Sjöqvist, D. M. Tong, and P. Zanardi, Phys. Rev. A **89**, 042302 (2014).
[14] G.-F. Xu and G.-L. Long, Sci. Rep. **4**, 6814 (2014).
[15] G. F. Xu, C. L. Liu, P. Z. Zhao, and D. M. Tong, Phys. Rev. A **92**, 052302 (2015).
[16] Z.-Y. Xue, J. Zhou, and Z. D. Wang, Phys. Rev. A **92**, 022320 (2015).
[17] Z.-Y. Xue, J. Zhou, Y.-M. Chu, and Y. Hu, Phys. Rev. A **94**, 022331 (2016).
[18] P. Z. Zhao, G. F. Xu, and D. M. Tong, Phys. Rev. A **94**, 062327 (2016).
[19] E. Herterich and E. Sjöqvist, Phys. Rev. A **94**, 052310 (2016).
[20] G. F. Xu, P. Z. Zhao, T. H. Xing, E. Sjöqvist, and D. M. Tong, Phys. Rev. A **95**, 032311 (2017).
[21] Z.-Y. Xue, F.-L. Gu, Z.-P. Hong, Z.-H. Yang, D.-W. Zhang, Y. Hu, and J. Q. You, Phys. Rev. Appl. **7**, 054022 (2017).
[22] G. F. Xu, P. Z. Zhao, D. M. Tong, and E. Sjöqvist, Phys. Rev. A **95**, 052349 (2017).
[23] P. Z. Zhao, G. F. Xu, Q. M. Ding, E. Sjöqvist, and D. M. Tong, Phys. Rev. A **95**, 062310 (2017).

- [24] Z.-P. Hong, B.-J. Liu, J.-Q. Cai, X.-D. Zhang, Y. Hu, Z. D. Wang, and Z.-Y. Xue, Phys. Rev. A **97**, 022332 (2018).
- [25] A. A. Abdumalikov, J. M. Fink, K. Juliusson, M. Pechal, S. Berger, A. Wallraff, and S. Filipp, Nature (London) **496**, 482 (2013).
- [26] D. J. Egger, M. Ganzhorn, G. Salis, A. Fuhrer, P. Mueller, P. K. Barkoutsos, N. Moll, I. Tavernelli, and S. Filipp, arXiv: 1804.04900.
- [27] Y. Xu, W. Cai, Y. Ma, X. Mu, L. Hu, T. Chen, H. Wang, Y.P. Song, Z.-Y. Xue, Z.-q. Yin, and L. Sun, arXiv: 1804.07591.
- [28] T. Yan, B.-J. Liu, K. Xu, C. Song, S. Liu, Z. Zhang, H. Deng, Z. Yan, H. Rong, M.-H. Yung, Y. Chen, and D. Yu, arXiv: 1804.08142.
- [29] G. Feng, G. Xu, and G. Long, Phys. Rev. Lett. **110**, 190501 (2013).
- [30] H. Li, L. Yang, and G. Long, Sci. China: Phys., Mech. Astron. **60**, 080311(2017).
- [31] C. Zu, W.-B. Wang, L. He, W.-G. Zhang, C.-Y. Dai, F. Wang, and L.-M. Duan, Nature (London) **514**, 72 (2014).
- [32] S. Arroyo-Camejo, A. Lazariev, S. W. Hell, and G. Balasubramanian, Nat. Commun. **5**, 4870 (2014).
- [33] Y. Sekiguchi, N. Niikura, R. Kuroiwa, H. Kano, and H. Kosaka, Nat. Photonics **11**, 309 (2017).
- [34] B. B. Zhou, P. C. Jerger, V. O. Shkolnikov, F. J. Heremans, G. Burkard, and D. D. Awschalom, Phys. Rev. Lett. **119**, 140503 (2017).
- [35] V. A. Mousolou, C. M. Canali, and E. Sjöqvist, New J. Phys. **16**, 013029 (2014).
- [36] V. A. Mousolou and E. Sjöqvist, Phys. Rev.A. **89**, 022117 (2014).
- [37] V. A. Mousolou, Phys. Rev. A **96**, 012307 (2017).
- [38] J. Zhang, S. J. Devitt, J. Q. You, and F. Nori, Phys. Rev. A **97**, 022335 (2018).
- [39] J. Koch, T. M. Yu, J. Gambetta, A. A. Houck, D. I. Schuster, J. Majer, A. Blais, M. H. Devoret, S. M. Girvin, and R. J. Schoelkopf, Phys. Rev. A **76**, 042319 (2007).
- [40] J. D. Strand, M. Ware, F. Beaudoin, T. A. Ohki, B. R. Johnson, A. Blais, and B. L. T. Plourde, Phys. Rev. B **87**, 220505(R) (2013).
- [41] M. Roth, M. Ganzhorn, N. Moll, S. Filipp, G. Salis, and S. Schmidt, Phys. Rev. A **96**, 062323 (2017).
- [42] M. Reagor *et al.* Sci. Adv. **4**, eaao3603 (2018).
- [43] X. Li, Y. Ma, J. Han, T. Chen, Y. Xu, W. Cai, H. Wang, Y. P. Song, Z.-Y. Xue, Z.-q. Yin, and L. Sun, arxiv: 1806.03886 .
- [44] J. Anandan, Phys. Lett. A **133**, 171 (1988).
- [45] J. Zhang, T. H. Kyaw, D.M. Tong, E. Sjöqvist, and L. C. Kwek, Sci. Rep. **5**, 18414 (2015).
- [46] M. H. Devoret and R. J. Schoelkopf, Science **339**, 1169 (2013).
- [47] C. Rigetti, *et al.* Phys. Rev. B **86**, 100506(R) (2012).
- [48] J. F. Poyatos, J. I. Cirac, and P. Zoller, Phys. Rev. Lett. **78**, 390 (1997).
- [49] A. Miranowicz, S. K. Özdemir, J. Bajer, G. Yusa, N. Imoto, Y. Hirayama, and F. Nori, Phys. Rev. B **92**, 075312 (2015).
- [50] R. Barends *et al.*, Nature (London) **508**, 500 (2014).